Evolution of spinon Fermi surface and magnetic response of hyperkagome spin liquids

Filomena Forte,[1,2] Jeroen van den Brink,[3] and Mario Cuoco[1,2,*]
[1]*CNR-SPIN, I-84084 Fisciano (SA), Italy*
[2]*Dipartimento di Fisica "E. R. Caianiello," Università di Salerno, I-84084 Fisciano (SA), Italy*
[3]*Institute for Theoretical Solid State Physics, IFW-Dresden, D-01171 Dresden, Germany*
(Received 20 August 2013; revised manuscript received 7 October 2013; published 25 October 2013)

Quantum spin liquids are elusive states of matter that are characterized by a lack of long-range magnetic order, which renders their *excitation spectra* the key to identifying them. Studying the magnetic response of a class of spin-liquid states with fermionic spinons and broken time reversal symmetry (TRS) on the three-dimensional hyperkagome lattice of $Na_4Ir_3O_8$, we demonstrate that the spinon Fermi surface has a topological transition as a function of the flux intensity generated by the spinons moving along loops within the unit cell. The spin dynamical structure factor reveals small pockets of gapped regions in energy and momentum existing below the topological transition and nondispersive high-intensity peaks which broaden when the TRS gets broken. These dynamical fingerprints closely track the nature of the spin-liquid ground state of $Na_4Ir_3O_8$.

DOI: 10.1103/PhysRevB.88.144422 PACS number(s): 75.10.Jm, 71.27.+a, 75.10.Kt

I. INTRODUCTION

The last decades have witnessed accelerating development in the research on quantum spin liquids (QSLs). QSLs can occur in magnetic materials where strong quantum fluctuations dominate the low-energy behavior, thereby fully suppressing the presence of any long-range magnetic order. There are more and more indications that this long-predicted state of quantum matter can also be realized experimentally.[1–4] An important and intriguing feature of QSLs is the presence of fractional ($S = 1/2$) neutral excitations in the form of spinons. Depending on the type of spin liquid, the spinons may obey Fermi or Bose statistics and may or may not have a mass gap. The most promising QSL candidate materials have frustrated lattices, in particular, of the pyrochlore, kagome, and hyperkagome type.[2,5] All these systems are insulating, have a high Curie-Weiss temperature, and yet show no ordering down to the lowest measured temperatures.

Here we consider the recently discovered $Na_4Ir_3O_8$, for which a number of theoretical proposals have been put forward to account for its intriguing phenomenology.[6–12] In particular, a critical spin liquid, with a spinon Fermi surface (SFS), has been invoked to address the nature and temperature evolution of its magnetic ground state.[8,9] The Ir^{4+} sublattice of $Na_4Ir_3O_8$ consists of a highly frustrated network of corner-sharing triangles: the hyperkagome lattice (Fig. 1). This hyperkagome lattice shares a local connectivity to the two-dimensional (2D) kagome, but it has several distinct features such as the three dimensionality and the structural chirality. This remarkable material is an insulator with a high Curie-Weiss temperature, $T_W = 650$ K, and a large effective moment, $p_{\text{eff}} = 1.96\mu_B$, yet does not exhibit any sign of magnetic order down to 2 K.[13] In particular, the puzzling behavior for the thermodynamic properties (e.g., the susceptibility and the specific heat) suggest that indeed an SFS might be realized in $Na_4Ir_3O_8$.[8,9]

From an experimental point of view, it is highly desirable to have access to such a QSL state in a way that goes beyond indirect macroscopic observations that point at gapless or gapful spectra of excitations. The intrinsically nonlocal nature of correlated QSL states, which have no unique static or periodic structure, makes them difficult to measure and characterize by the local or spatially averaged probes that are usually employed to determine ordered magnetic patterns. The signature of a QSL should however be present in its spectrum of excitations. This is illustrated by the 1D spin liquids, which have revealed their hallmark spinon-antispinon continuum in inelastic neutron scattering (INS)[14–16] and, more recently, in resonant inelastic x-ray scattering (RIXS).[17,18]

In this paper we demonstrate that there is a peculiar correlation between the excitations spectrum and the quantum nature of a class of 3D spin-liquid states with fermionic spinons on the hyperkagome lattice of $Na_4Ir_3O_8$. The SFS undergoes a topological transition when time-reversal symmetry (TRS) breaking occurs, as a function of the effective phase acquired by the spinons hopping on the lattice. The magnetic response, expressed via the spin dynamical structure factor (DSF), exhibits the following remarkable features: (i) small pockets in energy and momentum of gapped regions within the Brillouin zone, the presence and location of which are tuned by the strength of the flux field; (ii) a smooth reduction of the gapful regions by increasing the amplitude of the effective flux and changeover of the spectrum to completely gapless at the topological transition of the SFS; (iii) high-intensity nondispersive peaks at finite energies for a time-reversal-invariant state; and (iv) a significant broadening in the spectral weight in the presence of TRS breaking. These features, which are, in principle, directly accessible experimentally by INS or RIXS, represent the direct dynamical fingerprints of the QSL ground states on the 3D hyperkagome lattice and turn out to be very sensitive to the presence of any different type of additional TRS breaking.

II. MODEL AND SPINON ELECTRONIC STRUCTURE

Our starting point is a nearest-neighbor (NN) isotropic Heisenberg Hamiltonian on a hyperkagome lattice with antiferromagnetic exchange for $S = 1/2$, which has been shown to capture well the low-energy physics of $Na_4Ir_3O_8$.[5–10] After a suitable projection and decoupling, a spin-liquid state emerges that is captured by a Hamiltonian of fermionic spinons.[9,19,20] We consider quantum configurations that have the full $P4_132$ point group and translational symmetries but allow for

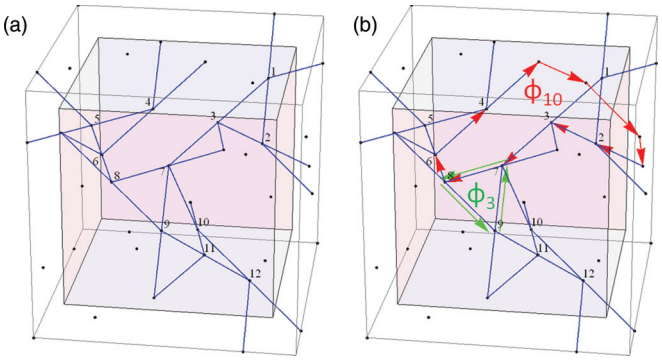

FIG. 1. (Color online) (a) Hyperkagome lattice formed by the iridium ions in $Na_4Ir_3O_8$. The inner cube represents the 12-site unit cell. Dark gray (blue) lines highlight the bonds between nearest-neighbor sites. (b) Illustration of a 10-site [black (red) arrows] and a 3-site [light-gray (green) arrows] elementary loop.

breaking TRS and are the solution of the Hamiltonian[9]

$$H = -\sum_{\langle i\alpha,j\beta\rangle,\sigma} t_{i\alpha,j\beta} c^{\dagger}_{i\alpha\sigma} c_{j\beta\sigma} + \text{H.c.} - \mu \sum_{i,\alpha\sigma} n_{i\alpha\sigma}, \qquad (1)$$

where i denotes the unit cell, α denotes sites in the unit cell, $\langle\cdots\rangle$ stands for a pair of NN sites, $c^{\dagger}_{i\alpha}(c_{j\alpha})$ denotes a fermionic spin creation (annihilation) operator, and $n_{i\alpha} = c^{\dagger}_{i\alpha} c_{i\alpha}$. The chemical potential μ is controlled so that the system is at half-filling (one spinon per site on average). Due to the point-group symmetry operations, the hyperkagome sites and bonds between NN sites are equivalent.[5,21] Consequently, one can assume the same hopping amplitude t on each bond, which, in the present theory, is related to the exchange constant J via the relation $t = \frac{3}{8} J |\sum_{\sigma} \langle c^{\dagger}_{i\alpha\sigma} c_{j\beta\sigma}\rangle|$, where E_0 is the ground-state energy and N_b is the number of bonds. We take J as the unit of energy hereafter.

Following the analysis in Ref. 9 we consider spin-liquid states where the spinon motion can be characterized by specific flux phases through closed loops on the hyperkagome lattice. A loop is defined by assigning a set of arrows to each bond, i.e., a global phase factor to the hopping integral $t_{i\alpha,j\beta} = |t| e^{-iA_{i\alpha,j\beta}}$, with $A_{i\alpha,j\beta} = -A_{,j\beta,i\alpha}$. The shortest loops on this lattice are triangles and decagons. In Fig. 1(b), these 3-site and 10-site directed loops are shown for a specific flux arrangement. For states that respect $P4_132$ and translational symmetries, the flux arrangement does not permit a net flux through the lattice and the 3-site and 10-site loops have the same flux, Φ_3 and Φ_{10}, respectively.[9] Moreover, any generic loop on a hyperkagome lattice can be decomposed into these two kinds of *elementary* loops. We specifically consider spin-liquid states that are distinguished from each other by the existence or absence of flux through the 10-site loop. The value of Φ_3 is then automatically fixed via the fundamental equation $2\Phi_3 = 3\Phi_{10} \text{mod}(2\pi)$. The only time-reversal-invariant symmetric state has $\Phi_3 = \Phi_{10} = 0$. However, when TRS is broken, configurations with arbitrary flux are allowed. We first analyze the case of uniform hopping and zero flux and then compare it with that of TRS-broken states. Since the unit cell of the hyperkagome lattice consists of 12 sites, the diagonalization of the Hamiltonian in Eq. (1) for $\Phi_{10} = 0$ yields 12 spin-degenerate bands, which are detailed

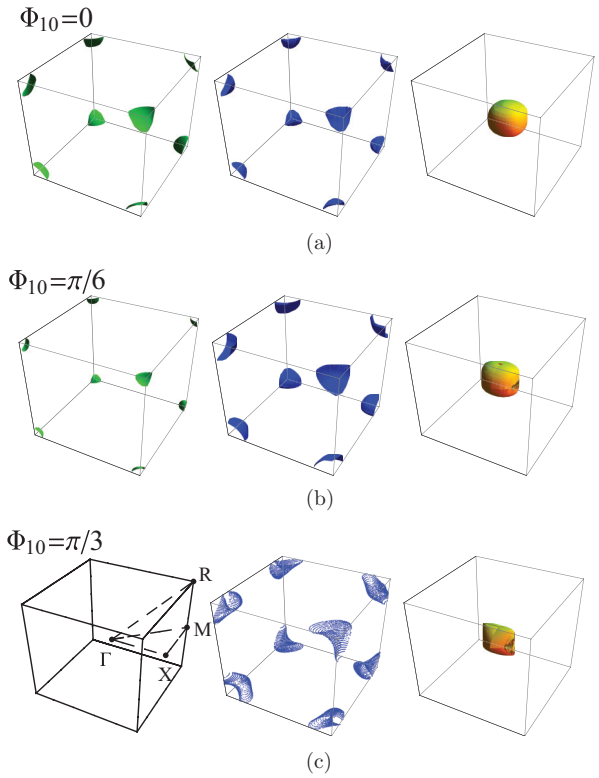

FIG. 2. (Color online) Spinon Fermi surfaces evaluated for value of the flux $\Phi_{10} = 0$ (a), $\Phi_{10} = \pi/6$ (b), and $\Phi_{10} = \pi/3$ (c).

in the Appendix. The resulting SFS at half-filling is illustrated in Fig. 2(a). It consists of two hole pockets around the R point of the cubic zone and one electron pocket around the Γ point. These surfaces are small and approximately spherical. The k_F vector for the electron surface along (1,0,0) is $\sim 0.31\pi/a$, while that of the hole pockets is $\sim 0.27\pi/a$.

All nonzero-flux states exhibit nontrival Fermi surfaces. With increasing values of Φ_{10}, different SFS topologies emerge for the various TRS states. In particular, it is possible to distinguish among two regimes, small-flux and large-flux behavior. Below the critical value $\Phi^c_{10} \sim \pi/6$, the topology of the SFS is very similar to the zero-flux phase. The k_F vector for the electron-like surface stays almost unchanged along (1,0,0), while it is slightly reduced along (1,1,1), thus leading to an enhanced asymmetry of the spherical surface. The Fermi volume of one hole surface is reduced with an increase in the flux and eventually vanishes at values greater than Φ^c_{10}.

Above Φ^c_{10}, an electronic topological transition takes place. There is still a sizable electron pocket around the Γ point, however, the spherical symmetry is completely lost and the volume is reduced with respect to the $\Phi_{10} = 0$ case. The remaining hole surface assumes a tubular shape around the R point, extending between $0.57\pi/a$ and π/a along (0,0,1). This is caused by the presence of smaller contiguous pockets around the R point with shallow energy dispersions. A breaking of TRS tends to lift many spinon band degeneracies and cause a general upwards shift of the bands in the high-energy sector (see the Appendix). As discussed later, these features are responsible for (i) a mild widening of the two-spinon bandwidth and (ii) a broadening of the peak structure in the two-spinon

response function, due to the increased number of allowed interband transitions.

III. SPIN DYNAMICAL STRUCTURE FACTOR

The magnetic excitation spectrum is deduced by computing the spin DSF $S(q,\omega)$ via the time- and spatial-dependent spin-spin correlation function

$$S(q,w) = \frac{1}{\pi}\mathrm{Im}\langle\psi_0|S_q^{z\dagger}\frac{1}{H+\omega-E_0-i\eta}S_q^z|\psi_0\rangle, \qquad (2)$$

where $|\psi_0\rangle$ and E_0 are the ground-state wave function and energy, $\eta \to 0^+$, and $S_q = \sum_i \exp^{iqR_i} S_i^z$ is the single-spin form factor. This quantity is directly accessible experimentally through INS, which can directly detect the spinon-antispinon continuum in 1D and 2D frustrated compounds.[14–16] Recently, it has been shown experimentally that also direct RIXS can give access to magnon and spinon excitations,[17,18,22,23] consistent with the theoretical predictions of Refs. 24–28. Spinons typically give rise to a highly dispersive continuum of excited states, the signature of the fractionalization of $S = 1$ excitations into multispinon excitations. The observed dominant scattering cross section is a two-spinon continuum, isotropic in spin space and extending between the dispersive lower boundary and the upper boundary, obtained by convolving the two spinons' energy branches. A characteristic feature is that most of the scattering weight is concentrated at the lower threshold, which follows a sinelike dispersion relation with period π. Moreover, the spectrum shows a strong momentum dispersion, with a maximum intensity observed at π/a. In the spin-liquid scenario employed for $Na_4Ir_3O_8$, $S(q,\omega)$ is calculated via the single spin form factor S_q,

$$S_q^z = \sum_k \sum_{r,s} M_{r,s}(k,k-q) d_{k-q,s}^\dagger d_{k,r}, \qquad (3)$$

where $d = Uc$, with U as the unitary matrix that diagonalizes the Hamiltonian of Eq. (1), and r and n are band indices. In writing Eq. (3), we have taken into account the isotropy in spin space and considered that, due to the spin degeneracy of the bands, one can omit the spin indices. The spin DSF is thus reduced to the particle-hole spectrum of the SFS, mediated by the matrix elements $M_{r,s}$, originating from the 12-site basis of the periodic cubic cell.

We now analyze in detail the magnetic spectrum starting from the zero-flux case. The calculated spectrum of excitations described by Eq. (3) is shown in Fig. 3. It consists of a broad continuum extending between $\omega/J = 0$ and $\omega/J = 1$, with dominant peaks located at $\omega/J = 0.3$, $\omega/J = 0.6$, and $\omega/J = 0.8$. Zooming in on the low-energy region of the spectrum, one can see that the threshold of the two-spinon continuum does not obey a well-defined momentum dispersion, but it varies along the different symmetry paths of the Brillouin zone. The spectrum is predicted to be gapless around Γ and R (see Fig. 3, left panels) and gapped around the X and M points as well as in the middle of the Γ-to-R direction. Particularly, the existence of an isotropic gapless region around Γ and R is directly connected to the topology of the SFS. Indeed, the approximately spherical electron and hole pockets located around these symmetry points ensure that gapless excitations are allowed for each q such that $|q| < 2k_F$. We also find that

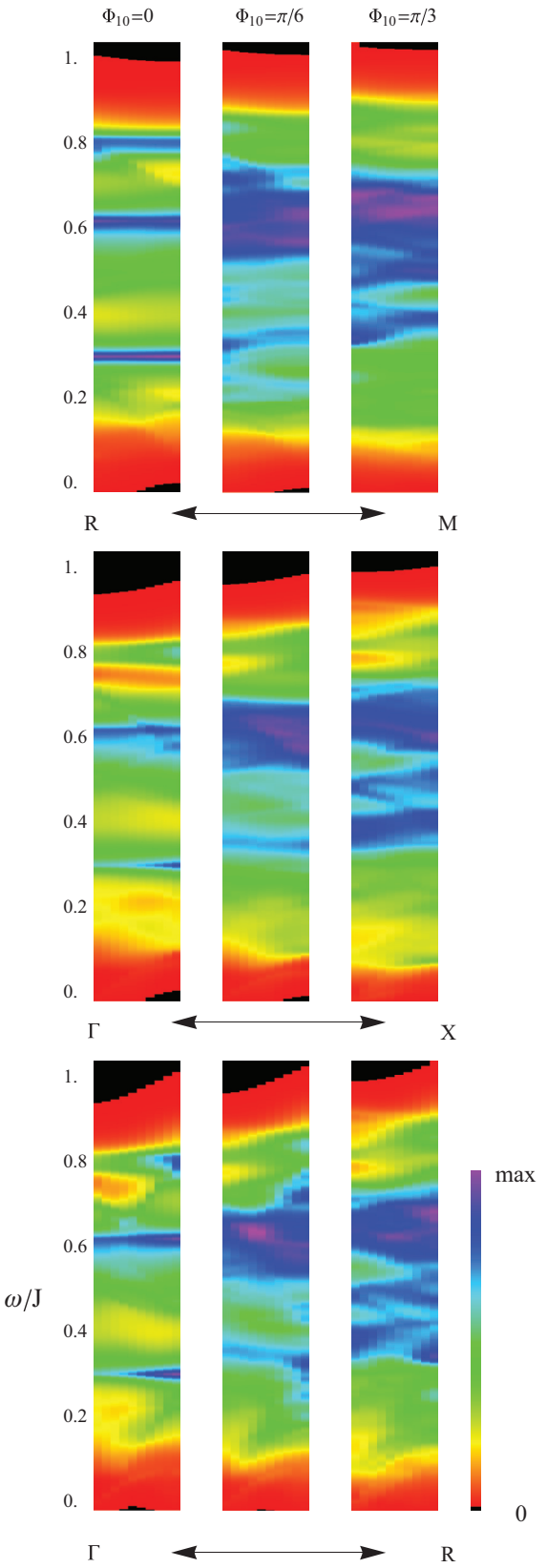

FIG. 3. (Color online) Spin dynamical structure factor of the Heisenberg model on a hyperkagome lattice along the main symmetry directions in the Brillouin zone, for the zero-flux state and nonzero-flux state with $\Phi_{10} = \pi/6$ and $\Phi_{10} = \pi/3$, respectively. The spectral intensity is rescaled to its maximum value for each flux case.

the excitation energy is almost independent of the transferred momenta q along the $\Gamma \rightarrow X$ and $R \rightarrow$ M paths, and it is only weakly dependent along the $\Gamma \rightarrow R$ path. These features comprise a fundamental difference with respect to the case of 1D systems with spinons, which exhibit well-defined bounds of the continuum, where the spectral weight piles up, and which, in addition, show a strong dispersion. It is remarkable that this feature explicitly does not occur for the spin-liquid states of $Na_4Ir_3O_8$.

Instead, the excitation spectrum strongly reflects the signatures of the presence of any flux phases. The two-spinon continuum for the nonzero flux states is reported in Fig. 3 for $\Phi_{10} = \pi/6$ [Fig. 3(b); center and right panels] and $\Phi_{10} = \pi/3$ [Fig. 3(c)], just below and above the critical flux, respectively. Nonzero flux phases produce a significant redistribution of the spectral weight. The spectra do not show well-defined peaks; in contrast, a broad continuum is observed, where most of the spectral weight is concentrated between about $\omega/J = 0.3$ and $\omega/J = 0.8$, with tails up to $\omega/J = 1.1$. Moreover, the momentum dispersion of the spectra is slightly affected by the flux. The broadening of the peak structure originates from the lifting of the band degeneracies and the increased number of allowed interband transitions, as discussed in the previous section. Below Φ_c, the SFS topology is similar to the zero-flux state. In this regime, the spectra show minor changes in the low-energy sectors with respect to the zero-flux state and we get gapful and gapless occurrence at the same points in the Brillouin zone. However, due to the anisotropy of the SFS, the gapless regions are substantially reduced in the TRS broken state. Above Φ_c, the energy window carrying most of the spectral weight is further restricted to the region $\omega/J = 0.4$–0.7. The spectrum is predicted to stay gapless around the Γ and the R point, also in the nonzero flux state, while it is turned from gapful to gapless around the X and M point. Thus the fingerprints of spin DSF can discriminate between zero- and non-zero-flux SFS states. As discussed above, these features are strictly related to the band structure and the topology of the SFSs, which in turn strongly depend on the flux state, particularly on the amplitude of the elementary 3-site and 10-site fluxes.

IV. CONCLUSIONS

We have determined the energy spectrum and the magnetic response of spin-liquid states with fermionic spinons on a 3D hyperkagome lattice in the presence of TRS breaking. Interestingly, the SFS changes its topology as a function of the flux amplitude, which has major consequences for the excitation spectrum. The evaluated spin DSF, for both unbroken and broken TRS states, consists of an almost-dispersionless spinon-antispinon continuum, extending up to an energy scale set by the magnetic exchange J. The low-energy sector is marked by gapped regions forming small energy and momentum pockets and located in specific points of the Brillouin zone that depend on the strength of the TRS breaking field. The threshold in energy for the gapped regions does not have a well-defined dispersion, which is in marked contrast to 1D spinon systems. We argue that the two-spinon spectral function measured by the spin DSF represents directly the SFS topology and can thus be used to distinguish between different SFS ground states with distinct TRS. INS and RIXS are, in principle, perfectly suited to test the predictions on the DSF presented here. One should note, however, that several theoretical and experimental indirect estimates[5,8,29] of the antiferromagnetic exchange assign a value to J in the range between 25 and 35 meV, which poses a major challenge for RIXS, which, at the iridium L edge, has at present an energy resolution of similar magnitude, whereas INS experiments will require a relatively large mass of single crystals of neutron-absorbing $Na_4Ir_3O_8$.

ACKNOWLEDGMENTS

We thank John Hill, Xuerong Liu, Des McMorrow, and Mark Dean for fruitful discussions. The research leading to these results received funding from FP7/2007-2013 under Grant No. 264098–MAMA.

APPENDIX

In this Appendix we present the electronic structure of a class of QSL states with fermionic spinons on a hyperkagome lattice, which are characterized by effective flux phases acquired by the spinons moving through closed loops on the lattice. We compute the spinon electronic structure for QSL states that are solutions of the Hamiltonian of fermionic spinons, Eq. (1),[9,19,20] allowing for breaking of TRS. Only the hopping between each site and its four NNs is considered, and the spinon motion is characterized by specific flux phases through closed loops on the hyperkagome lattice according to the prescriptions in Ref. 9. The chemical potential μ is selected so that the system is at half-filling (one spinon per site on average).

By diagonalizing the Hamiltonian, 12-spin degenerate bands can be found, which are shown in Figs. 4(a) and 4(b) for the case of zero flux and nonzero flux, respectively. Here, the reference energy is the chemical potential μ, which must be determined for each flux phase. All the energies are expressed

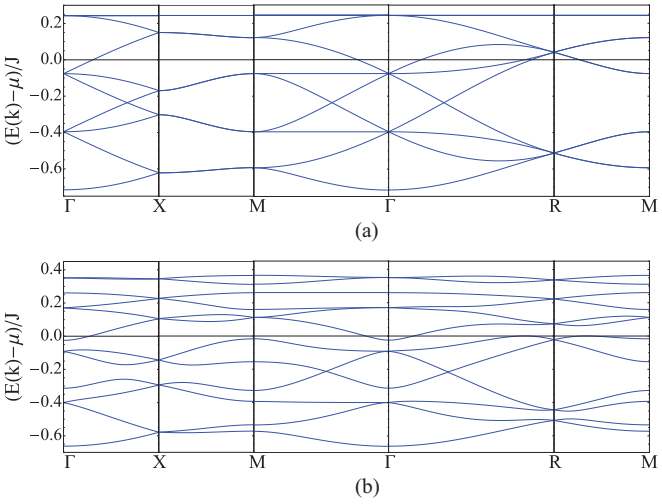

FIG. 4. (Color online) Spinon electronic structure for $\Phi_{10} = 0$ (a) and $\Phi_{10} = \pi/3$ (b) flux states. Energy is scaled to the exchange constant J. The chemical potential μ is taken as the reference energy.

in units of J, according to the relation $t = \frac{3}{8} J |\sum_{\sigma} \langle c^{\dagger}_{i\alpha\sigma} c_{j\beta\sigma} \rangle|$, where E_0 is the ground-state energy and N_b is the number of bonds. This relation reduces to $t \sim 0.16\,\mathrm{J}$ for all the considered flux states.

In Fig. 4(a), the case of zero flux and a time-reversal-invariant state is reported. When the spin degeneracy is neglected, one can distinguish between eight nondegenerate bands, and four degenerate bands at the high top of the spectrum. Particularly, bands 5, 6, and 7 have a distinct structure and cross the chemical potential, giving rise to an electron pocket around the Γ point and hole pockets around the R point.

The electronic structure for a TRS-broken state with $\Phi_{10} = \pi/3$ is reported in Fig. 4(b). As one can see, nonzero-flux phases allow for the lifting of many of the band degeneracies in Fig. 4(a), although some residual degeneracy is left at the high-symmetry points and at the top end of the spectrum. We also note that the flat bands shown in Fig. 4(a) have now acquired a finite dispersion. Moreover, there occurs an upwards shift of the bands in the high-energy sector. These features are responsible for (i) a mild widening of the two-spinon bandwidth and (ii) a broadening of the peak structure in the two-spinon response function, due to the increased number of allowed interband transitions.

*marcuo@sa.infn.it

[1] P. A. Lee, Science **321**, 1306 (2008).
[2] L. Balents, Nature **464**, 16361 (2010).
[3] Y. Shimizu, K. Miyagawa, K. Kanoda, M. Maesato, and G. Saito, Phys. Rev. Lett. **91**, 107001 (2003).
[4] M. P. Shores, E. A. Nytko, B. M. Bartlett, and D. G. Nocera, J. Am. Chem. Soc. **127**, 13462 (2005).
[5] G. Chen and L. Balents, Phys. Rev. B **78**, 094403 (2008).
[6] J. M. Hopkinson, S. V. Isakov, H. Y. Kee, and Y. B. Kim, Phys. Rev. Lett. **99**, 037201 (2007).
[7] M. J. Lawler, H.-Y. Kee, Y. B. Kim, and A. Vishwanath, Phys. Rev. Lett. **100**, 227201 (2008).
[8] M. J. Lawler, A. Paramekanti, Y. B. Kim, and L. Balents, Phys. Rev. Lett. **101**, 197202 (2008).
[9] Y. Zhou, P. A. Lee, T.-K. Ng, and F.-C. Zhang, Phys. Rev. Lett. **101**, 197201 (2008).
[10] E. J. Bergholtz, A. M. Lauchli, and R. Moessner, Phys. Rev. Lett. **105**, 237202 (2010).
[11] Y. Zhang, T. Grover, and A. Vishwanath, Phys. Rev. Lett. **107**, 067202 (2011).
[12] G. Chen and Y. B. Kim, Phys. Rev. B **87**, 165120 (2013).
[13] Y. Okamoto, M. Nohara, H. Aruga-Katori, and H. Takagi, Phys. Rev. Lett. **99**, 137207 (2007).
[14] B. Lake, D. A. Tennant, C. D. Frost, and S. E. Nagler, Nat. Mater. **4**, 329 (2005).
[15] A. C. Walters, T. G. Perring, J.-S. Caux, A. T. Savici, G. D. Gu, C.-C. Lee, W. Ku, and I. A. Zaliznyak, Nat. Phys. **5**, 867 (2009).
[16] R. Coldea, D. A. Tennant, and Z. Tylczynski, Phys. Rev. B **68**, 134424 (2003).
[17] S. Glawion, J. Heidler, M. W. Haverkort, L. C. Duda, T. Schmitt, V. N. Strocov, C. Monney, K. J. Zhou, A. Ruff, M. Sing, and R. Claessen, Phys. Rev. Lett. **107**, 107402 (2011).
[18] J. Schlappa, K. Wohlfeld, K. J. Zhou, M. Mourigal, M. W. Haverkort, V. N. Strocov, L. Hozoi, C. Monney, S. Nishimoto, S. Singh, A. Revcolevschi, J.-S. Caux, L. Patthey, H. M. Rnnow, J. van den Brink, and T. Schmitt, Nature **485**, 82 (2012).
[19] P. A. Lee, N. Nagaosa, and X. G. Wen, Rev. Mod. Phys. **78**, 17 (2006).
[20] X.-G. Wen, *Quantum Field Theory of Many-Body Systems* (Oxford Graduate Texts, New York, 2004).
[21] T. Hahn, *International Tables for Crystallography, Vol. A. Space Group Symmetry*, 4th ed. (Kluwer Academic, Dordrecht, 1996).
[22] J. Kim, D. Casa, M. H. Upton, T. Gog, Y.-J. Kim, J. F. Mitchell, M. van Veenendaal, M. Daghofer, J. van den Brink, G. Khaliullin, and B. J. Kim, Phys. Rev. Lett. **108**, 177003 (2012).
[23] X. Liu, Vamshi M. Katukuri, L. Hozoi, W.-G. Yin, M. P. M. Dean, M. H. Upton, J. Kim, D. Casa, A. Said, T. Gog, T. F. Qi, G. Cao, A. M. Tsvelik, J. van den Brink, and J. P. Hill, Phys. Rev. Lett. **109**, 157401 (2012).
[24] L. J. P. Ament, G. Ghiringhelli, M. M. Sala, L. Braicovich, and J. van den Brink, Phys. Rev. Lett. **103**, 117003 (2009).
[25] J. Luo, G. T. Trammell, and J. P. Hannon, Phys. Rev. Lett. **71**, 287 (1993).
[26] M. W. Haverkort, Phys. Rev. Lett. **105**, 167404 (2010).
[27] L. J. P. Ament, G. Khaliullin, and J. van den Brink, Phys. Rev. B **84**, 020403(R) (2011).
[28] M. van Veenendaal, arXiv:1106.0640v1.
[29] M. R. Norman and T. Micklitz, Phys. Rev. B **81**, 024428 (2010).